RSC Advances

REVIEW

View Article Online
View Journal | View Issue

Open Access Article. Published on 26 July 2023. Downloaded on 1/23/2026 1:45:14 AM.
This article is licensed under a Creative Commons Attribution-NonCommercial 3.0 Unported Licence.

Check for updates

Cite this: *RSC Adv.*, 2023, **13**, 22579

The mathematical catalyst deactivation models: a mini review

Zaidoon M. Shakor*[a] and Emad N. Al-Shafei *[b]

Received 2nd May 2023
Accepted 12th July 2023

DOI: 10.1039/d3ra02912c

rsc.li/rsc-advances

Catalyst deactivation is a complex phenomenon and identifying an appropriate deactivation model is a key effort in the catalytic industry and plays a significant role in catalyst design. Accurate determination of the catalyst deactivation model is essential for optimizing the catalytic process. Different mechanisms of catalyst deactivation by coke and metal deposition lead to different deactivation models for catalyst activity decay. In the rigorous mathematical models of the reactors, the reaction kinetics were coupled with the deactivation kinetic equation to evaluate the product distribution with respect to conversion time. Finally, selective and nonselective deactivation kinetic models were designed to identify catalyst deactivation through the propagation of heterogeneous chemical reactions. Therefore, the present review discusses the catalyst deactivation models designed for CO_2 hydrogenation, Fischer–Tropsch, biofuels and fossil fuels, which can facilitate the efforts to better represent the catalyst activities in various catalytic systems.

1. Introduction

All catalytic processes suffer from a decrease in catalytic activity with operation time which greatly affects process stability and consequently decreases the yield and selectivity of the desired products. The time taken by loss of catalyst activity varies from a few seconds during the fluidized catalytic cracking (FCC) process to a few years during hydrodesulfurization (HDS). Accordingly, the rate of catalyst deactivation depends on the process conditions, catalyst type, reactant concentrations and contaminant with feed presence.[1–3] Catalyst deactivation is classified by process type as thermal, mechanical, or chemical and by mechanisms such as fouling,[4–6] poisoning,[7] vapor formation, thermal degradation,[8] attrition/crushing,[9] vapor–solid and solid–solid reactions.[10] The thermal degradation and poisoning are generally slow and irreversible, whereas coke fouling is rapid and reversible.[11] Catalyst deactivation models

[a]*Chemical Engineering Department, University of Technology, Baghdad, Iraq. E-mail: Zaidoon.M.Shakor@uotechnology.edu.iq*

[b]*Research and Development Center, Saudi Aramco, Dhahran 31311, Saudi Arabia. E-mail: Emad.Shafei@aramco.com*

Prof. Dr Zaidoon M. Shakor is a faculty member in the Chemical Engineering Department, University of Technology. He held a BSc (1997), MSc (1999) and PhD (2004) in chemical engineering from the Chemical Engineering Department of the University of Technology, Iraq. Experience in reaction kinetics modeling from small to large scale industrial catalytic processes. Experience in catalyst synthesis, reactive distillation, azeotropic and extractive distillation, adsorption, modeling, simulation and computational fluid dynamics (CFD). He is a specialist in applying modern simulation software such as MATLAB and HYSYS to improve the performance of chemical engineering processes.

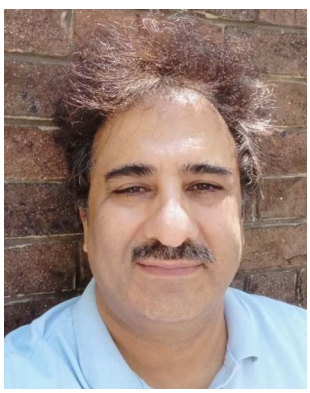

Dr Emad Al-Shafei, a research consultant at the Research and Development Center, Saudi Aramco, Dhahran KSA. He received a PhD in Chemistry (Catalysts) from the University of Huddersfield (United Kingdom), and an MSc in Analytical Chemistry, and BSc Chemistry with Chemical Engineering from the same university. His research interest focused on catalyst development & characterization, catalytic reaction, industrial catalysts, carbon dioxide utilization for petrochemicals, dry reforming for decarbonization, nano zeolite development, and steam catalytic cracking for heavy hydrocarbons to olefins.

© 2023 The Author(s). Published by the Royal Society of Chemistry

Open Access Article. Published on 26 July 2023. Downloaded on 1/23/2026 1:45:14 AM.
This article is licensed under a Creative Commons Attribution-NonCommercial 3.0 Unported Licence.

can be categorized into selective and non-selective models according to the mechanism of loss of the active sites of the catalyst. In non-selective deactivation, the rate of active sites consumption depends on the time-on-stream (TOS) only, whereas in selective deactivation, the components of the reaction mixture are affected individually by the rate of consumption/generation of the active sites.

Hundreds of models have been applied to evaluate catalyst activity in the past eighty years, although some of these models are simple as a function of time, while others are more sophisticated as a function of multi deactivation variables.[12] Voorhies *et al.*[13] reported a simple power-law correlation for modeling the catalyst deactivation proportional to the amount of coke deposited. Similarly, an exponential form of the catalyst deactivation model developed by Weekman *et al.*[14] was designed to characterize the catalyst activity during gas oil cracking (VGO) in a fixed-bed reactor. Dumez and Froment[15] investigated five catalyst deactivation models, in which the catalyst deactivation function was multiplied by the intrinsic reaction rate to estimate the net reaction rate. While a semi-empirical relationship was studied to determine the dependency of the number of active sites on the coke content, Devoldere and Froment[16] studied four models to characterize catalyst deactivation from coke formation over K–FeO based catalyst applied at the industrial scale level for ethylbenzene dehydrogenation. Nazarova *et al.*[17] developed a mathematical model for fluidized catalytic cracking (FCC) considering the deactivation of zeolite catalyst by coke and heavy metals, such as V and Ni. The exponential form of the catalyst deactivation model was also studied to correlate the catalyst activity with the coke content. The instantaneous amount of coke was estimated by solving a differential equation based on the hydrocarbon conversion mechanisms. Ebrahimi *et al.*[18] applied a nine-lumped kinetic model to represent the catalytic cracking of vacuum gas oil (VGO) and used the exponential formula of time-on-stream (TOS) and temperature to describe catalyst deactivation. Cordero-Lanzac *et al.*[19] applied a complex reaction networks methodology of fast catalyst deactivation to simulate the methanol-to-olefins (MTO) process with different reactor configurations. The proposed deactivation kinetics were found to depend on the concentrations of the oxygenated and carbon-containing product in the reaction medium. Shakor *et al.*[20] simulated an industrial scale heavy naphtha reforming process using a kinetic model involving 32 lumps and 132 reaction routes and applied first order for the catalyst deactivation rate. Despite this observation, the catalytic activity decayed to 59% of its initial value after 1225 days of operating.

The deactivation model of a catalyst plays a significant role in process simulation, reactor design and control of industrial catalytic reactors. However, several review papers[10,21–25] have been published in the past few years, and specific experimental studies on catalyst deactivation for specific chemical processes have been discussed.[26,27] Therefore, the present review discusses the mathematical models of catalyst deactivation designed for CO_2 hydrogenation, Fischer–Tropsch, biofuels and fossil fuels which can facilitate efforts for a broader representation to comprehend the catalyst activities in current catalytic chemical processes.

2. Catalyst deactivation models

Catalyst deactivation models are either algebraic or differential expressions that correlate changes in the catalyst activity with the reaction. The catalyst activity at any time "t" is equal to a ratio of the reaction rate at any given time "t" and the reaction rate applies to fresh catalyst[28] as described in eqn (1).

$$a(t) = \frac{\text{Reaction rate at time}(t = t)}{\text{Reaction rate at time}(t = 0)} \tag{1}$$

The initial reaction rate was measured at zero time point. Different models have been proposed in the literature to represent catalyst deactivation depending on the time-on-stream (TOS) of hydrocracking catalysts,[28] the coke content of fluidized catalytic cracking catalysts,[29] the operating conditions of the Fischer–Tropsch catalyst[30] and the reaction mixture with two-step deactivation of reversible and irreversible models.[31] These models are theoretical, empirical, or semi-empirical, and the most relevant deactivation model is summarized in the following sections.

2.1 Time dependent catalyst deactivation model

Catalyst activity decays with time, resulting in the reduction of active sites on the catalyst surface. The time-on-stream definition has been extensively applied to express approximate deactivation mechanisms. These expressions utilizes either exponential or power law and vary in deactivation order and functionality with respect to the time-on-stream. Voorhies *et al.*[13] studied catalyst deactivation in fluidized catalytic cracking *via* coke formation (Fig. 1) and applied the earliest empirical catalyst activity model described in eqn (2).

$$a(t) = At^n \tag{2}$$

The order of catalyst decay depends on the catalyst and feedstock type.[32] Ozawa *et al.*[33] studied PdO/Al_2O_3 with additive of La and Nd catalyst deactivation at 850 °C, during CH_4 oxidation in a fixed-bed reactor at atmospheric pressure. They observed that the catalyst was deactivated by the rapid transformation of oxidation state from PdO to metallic Pd with slow

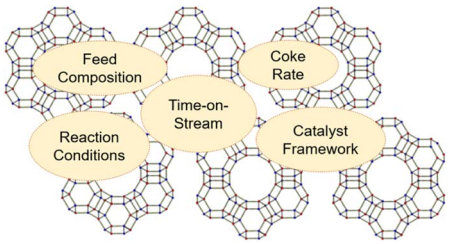

Fig. 1 Catalyst deactivation of fluidized catalytic cracking catalysts.

 © 2023 The Author(s). Published by the Royal Society of Chemistry

Open Access Article. Published on 26 July 2023. Downloaded on 1/23/2026 1:45:14 AM.
This article is licensed under a Creative Commons Attribution-NonCommercial 3.0 Unported Licence.

particle agglomeration. Accordingly, two-term deactivation mathematical models were attributed to evaluate the catalyst activity during the reaction as described in eqn (3).

$$a(t) = r_1[1/(1-\alpha_1 t)]^{n_1} + r_2[1/(1-\alpha_2 t)]^{n_2} \quad (3)$$

where "r", "α" and "n" are constants, subscripts 1 and 2 are the rapid and slow deactivation species respectively and "t" is time on a stream. Table 1 lists the catalyst deactivation models based on the time-on-stream (TOS). The main drawback of these models is that they do not take into consideration the effects of the reaction temperature, pressure and amount of coke formed over the catalyst.[34] This type of deactivation model is appropriate for systems with fast catalyst deactivation such as fluidized catalytic cracking catalysts[35–38] and catalyst used for biofuel from biomass fermentation.[39] The catalyst activity depends more on the effect of the deactivation rate over time, than on the temperature and reactant concentrations.

2.2 Temperature dependent catalyst deactivation model

Catalyst deactivation increases with time and temperature during catalytic reactions. Subsequently, increasing the severity of the reaction system leads to faster coke deposition and catalyst deactivation, in which temperature has the strongest effect on the reaction rate and consequently catalyst deactivation. The exponential function is shown in eqn (4) has rarely been used to model the deactivation of fluidized catalytic cracking and biomass-derived chemical.[18,43] Whereas the catalyst deactivation coefficient (α) attributes as a function of temperature using the Arrhenius-type as described in eqn (5). The Arrhenius-type expression was used to express the effect of temperature on the catalyst deactivation coefficient as shown in eqn (6).

$$a = \alpha_o e^{-\alpha t_{os}} \quad (4)$$

$$\alpha = \alpha_o e^{-\left(\frac{E_\alpha}{RT}\right)} \quad (5)$$

$$k_d = k_{do}\exp\left(\frac{-E_d}{RT}\right) \quad (6)$$

A generalized power-law model (eqn (7)) has been extensively applied to represent catalyst deactivation.[44–49] Accordingly, by taken deactivation power as either a "1" or "2" through integration eqn (7), the algebraic expressions for catalyst activity can be achieved as shown in eqn (8) and (9) respectively:

$$-\frac{da}{dt} = k_d a^n \quad (7)$$

$$a = e^{-k_d t} \text{ for } n = 1 \quad (8)$$

$$a = \frac{1}{1+k_d t} \text{ for } n = 2 \quad (9)$$

In addition, Chen and Lua[50] added the term residence time to the power-law deactivation model as shown in eqn (10). Bartholomew[51] confirmed that a generalized power-law expression (GPLE) with residual activity was represented by catalyst deactivation, which was enhanced compared to the power-law expression. The GPLE catalyst deactivation model is shown in eqn (11), and has been proposed by several authors, mainly for Fe–Co oxide catalysts in Fischer–Tropsch which deactivated from carbidization, change of metal oxidation state and carbon formation during hydrogenation reactions.[51–54]

$$\frac{da}{dt} = -k_{do} e^{-\left(\frac{E_d}{RT}\right)} a^n t_R{}^m \quad (10)$$

$$\frac{da}{dt} = -k_d\left(a - a_{eq}\right)^m \quad (11)$$

Residual activity "a_{eq}" is achieved when a balance is established between the rate of deactivation and the rate of self-generation for active sites.[55] Accordingly, the deactivation model derived by Honken,[56] shown in eqn (12), was found to be

Table 1 Time dependent catalyst deactivation model of fuel catalyst systems

Deactivation model	Catalyst	TOS[a]	Reactor Type	Reaction system	Reference
$a = At^n$	Silica–alumina	300 min	Fixed bed reactor	Catalytic cracking of gas oils	Voorhies[13]
$a = \alpha t_{os}{}^{-n}$	FCC catalyst	0–4 s	Riser reactor	Gas oil cracking	Theologos & Markatos[35]
$a = \frac{1}{1+\beta t_{os}{}^n}$	FCC catalyst	nt[b]	Commercial fluidized catalytic cracking reactor	Vacuum gas oil cracking	Rainer *et al.*[36]
	FCC catalyst	0–5 s	Industrial fluidized catalytic cracking reactor	Catalytic cracking of vacuum residue	Olafadehan, *et al.*[37]
$a = e^{-\alpha t_{os}}$	Ni/MgO	18 h	Fixed bed reactor	Hexane reforming	Trunfio & Arena[40]
	HZSM-5, beta, and Y-zeolite	nt[b]	Fluidized bed reactor	Catalytic pyrolysis of gas oils	Zhang *et al.*[38]
$a = e^{-\alpha t_{os}{}^n}$	FCC catalyst	0.03–0.09 s	Plug flow reactor	Gas oil cracking	Hagelberg *et al.*[41]
	Pt-based catalyst	40 h	Membrane reactor	Propane dehydrogenation	Ricca *et al.*[42]
$a = \exp(-k_d t)$	Pd/MWCNT + HZSM-5	5 h	Plug flow reactor	Biofuel: biomass fermentation	Jadon *et al.*[39]

[a] TOS: time-on-stream. [b] Not reported.

Open Access Article. Published on 26 July 2023. Downloaded on 1/23/2026 1:45:14 AM.
This article is licensed under a Creative Commons Attribution-NonCommercial 3.0 Unported Licence.

Table 2 Temperature dependent catalyst deactivation model

Deferential form	Integral form	Catalyst	TOS	Reactor type	Reaction	Reference
nt[a]	$a = e^{-\alpha t_{os}}$	FCC catalyst	90 s	Fixed bed reactor	VGO catalytic cracking	Ebrahimi *et al.*[18]
	$\alpha = \alpha_o e^{-\left(\frac{E_\alpha}{RT}\right)}$	FCC catalyst	nt[a]	Fixed and fluidized bed	VGO pyrolysis	Naik *et al.*[43]
nt[a]	$a = (1 - k_d t)$	Pt/Al_2O_3	nt[a]	Fixed bed reactor	Dehydrogenation methylcyclohexane	Usman *et al.*[69]
$-\frac{da}{dt} = k_d a$	$a = e^{-k_d t}$	Pt–Sn/Al_2O_3	100 h	Fixed bed reactor	Propane dehydrogenation	Zangeneh *et al.*[44]
		nt[a]	10–10000 h	Packed-bed reactor	Hydrogenation of CO_2	Sun *et al.*[45]
		FCC catalyst	2–10 s	FCC reactor	Vacuum gas oil (VGO) catalytic cracking	Sani *et al.*[46]
		TS-1/SiO_2	1–24 h	Fixed-bed reactor	Epoxidation of allyl chloride with hydrogen peroxide	Lin *et al.*[47]
		nt[a]	nt[a]	Fixed-bed reactor	Ethanol dehydration	Demuner *et al.*[48]
		Pt/Al_2O_3	1225 day	Fixed bed reactor	Heavy naphtha reforming	Shakor *et al.*[20]
$-\frac{da}{dt} = k_d a^2$	$a = \frac{1}{1 + k_d t}$	Pd–Ag/a-Al_2O_3	120 h	Fixed bed reactor	Selective hydrogenation of acetylene to ethylene	Ravanchi *et al.*[49]
$-\frac{da}{dt} = k_d a^2$	$a = \frac{1}{1 + k_d t}$	Cu/AC	12 h	Fixed bed reactor	Acetylene hydrochlorination	Xu *et al.*[70]
nt[a]	$a = \frac{1}{(1 + k_d t)^m}$	NiMo/Al_2O_3	0–550 h	Continuous stirred tank basket reactor (CSTBR)	Hydrocracking of heavy oil	Martínez and Ancheyta[67]
$-\frac{da}{dt} = k_d a^n$	$a(t) = [1 + k_d(n-1)t]^{\frac{-1}{n-1}}$	H_2O_2 with TS-1/SiO_2	0–50 h	Fixed-bed reactor	Liquid phase propylene epoxidation	Feng *et al.*[71]
		Nanocrystalline zeolite beta	0–6 h	Fixed-bed micro-reactor	Catalytic cracking of used palm oil	Taufiqurrahmi *et al.*[72]
		Pd/carbon	0–400	Fixed bed reactor	Crude terephthalic acid hydro-purification	Li *et al.*[73]
		Ni–Al oxide	0–165 h	Fixed bed reactors	CO_2 methanation	Ewald *et al.*[65]
		brewer's spent yeast (BSY)	120 min	Batch reactor	Biodiesel production from FFA	Arumugamurthy *et al.*[66]
		Ni based catalyst	0–900 day	Membrane reformer	Methane reforming	Jokar *et al.*[74]
		Ni/Al_2O_3	0–100 h	Fixed bed reactors	CO_2 methanation	Morosanu *et al.*[75]
		HY-zeolites	5 min	Packed bed reactor	Dehydration of glycerol to acrolein	Pala-Rosas *et al.*[76]
$\frac{da}{dt} = -k_{do} e^{-\left(\frac{E_d}{RT}\right)} a^n t_R{}^m$	nt[a]	SBA-15	500 min	Fixed bed reactor	Methane decomposition	Chen and Lua[50]
$-\frac{da}{dt} = k_d(a - a_\infty)^n$	nt[a]	Pt/Al_2O_3	0–350 h	nt[a]	nt[a]	Bartholomew[51]
$-\frac{da}{dt} = k_d(a - a_\infty)$	$a = a_\infty + (1 - a_\infty)e^{-k_d t}$	Cobalt based catalyst	0–1000 h	Bubble-column reactor	Fischer–Tropsch	Argyle *et al.*[52]
		Chiral	0–242.2 h	Batch reactor	Hydrogenation of acetophenone	Ruelas-Leyva & Fuentes[53]
$-\frac{da}{dt} = k_d(a - a_\infty)^2$	$a = \frac{1}{-k_d t + \frac{1}{(1 - a_\infty)}} + a_{ss}$	Fe/Al_2O_3	0–1300 h	Slurry bubble column reactor	Fischer–Tropsch	Ghofran *et al.*[54]
$-\frac{da}{dt} = k_{do} e^{-\frac{E_d}{R}\left(\frac{1}{T} - \frac{1}{T_R}\right)} a^5$	nt[a]	$CuO/ZnO/Al_2O_3$	nt[a]	nt[a]	nt[a]	Honken[56]
$-\frac{da}{dt} = k_{do} e^{-\frac{E_d}{R}\left(\frac{1}{T} - \frac{1}{T_R}\right)} a^7$	nt[a]	Pt/Re/Al_2O_3	0–800 day	Spherical packed-bed reactor	Naphtha reforming	Rahimpour *et al.*[64]
	nt[a]	Pt/Re/Al_2O_3	0–800 day	Spherical packed-bed reactor	Naphtha reforming	Iranshahi *et al.*[68]

[a] Not reported.

© 2023 The Author(s). Published by the Royal Society of Chemistry

Open Access Article. Published on 26 July 2023. Downloaded on 1/23/2026 1:45:14 AM. This article is licensed under a Creative Commons Attribution-NonCommercial 3.0 Unported Licence.

suitable for representing the catalyst deactivation in many industrial scale applications.[57–63] Rahimpour *et al.*[64] applied a seventh-order catalyst deactivation model to study the dynamic catalyst deactivation from carbonic coke formation during naphtha reforming reactions at 502–504 °C and pressure 34–37 bar, in which carried out in a radial flow spherical reactor as shown in eqn (13).

$$-\frac{\mathrm{d}a}{\mathrm{d}t} = k_{\mathrm{do}}\exp\left[\frac{E_{\mathrm{d}}}{R}\left(\frac{1}{T_{\mathrm{o}}} - \frac{1}{T}\right)\right]a^5 \tag{12}$$

$$-\frac{\mathrm{d}a}{\mathrm{d}t} = k_{\mathrm{do}}\exp\left[\frac{E_{\mathrm{d}}}{R}\left(\frac{1}{T_{\mathrm{o}}} - \frac{1}{T}\right)\right]a^7 \tag{13}$$

Temperature dependent catalyst deactivation models are presented in Table 2. These models are algebraic and/or differential forms of catalyst deactivation and are applied to deactivation of nickel catalyst from coke during CO_2 hydrogenation to methane,[65] biofuel,[66] iron and cobalt in the Fischer–Tropsch[52] catalytic deactivation reactions. For dynamic processes, the differential arrangements of the catalyst deactivation model of reforming[20] and hydrocracking catalysts[67] are slightly more accurate than those of algebraic route because these models represent instantaneous changes in catalyst activity.[64,68]

2.3 Coke formation dependent catalyst deactivation model

Coke deposition has been proven to be the main reason for catalyst deactivation in catalytic industrial processes, owing to the blocking of the active pore sites of the catalyst. The coke formation rate in the catalyst depends on the feed composition, reaction conditions (516–568 °C) and time-on-stream of propane dehydrogenation at atmospheric pressure using Pt/Al and Pt–Sn/Al oxide catalysts.[77] Coking at low temperatures was found to result in higher coke accumulation during catalytic cracking over β-zeolite catalyst at reaction temperature 400–500 °C, used for biofuel than that at higher temperatures, and the lower temperature conversion was attributed to the higher rate of condensation of coke components.[72] Catalyst deactivation by coke formation, occurs through a reversible or an irreversible mechanism. The presence of hydrogen in the naphtha reformer unit operated at 507–548 °C and pressure 1.5 bar, contributes to the removal of reversible coke and anticipated to decrease the catalyst deactivation rate.[78]

A modern catalytic cracking model uses a negative exponential function to represent the fluidized catalytic cracking of zeolite catalyst and coke deactivation.[79–82] The coke content has an inverse effect on the active pore sites inside the catalyst particles. Therefore, several researchers have studied the relationship between catalyst activity and coke content over Ni–Ce/Al oxide as dry reforming catalysts, as shown in eqn (14).[83–85] Froment *et al.*[26] described dependence of the catalyst activity on the coke formation during 1-butene dehydrogenation at 560–600 °C as shown in eqn (15). Additionally, Dumez and Froment[15] proposed five forms of deactivation function depends on carbon content over 20% Cr/Al oxide catalyst for the dehydrogenation of 1-butene to butadiene at 490–600 °C and pressure 0.2–2.7 bar, these deactivation forms are shown in eqn (17)–(21).

$$a = \left(1 - \frac{C_{\mathrm{c}}}{C_{\mathrm{c,max}}}\right)^2 \tag{14}$$

$$a = \frac{C_{\mathrm{c,max}} - C_{\mathrm{c}}}{C_{\mathrm{c,max}}} \tag{15}$$

$$a = 1/(1 + \alpha C_{\mathrm{C}})^n \tag{16}$$

$$a = \exp(-\alpha C_{\mathrm{C}}) \tag{17}$$

$$a = 1 - \alpha C_{\mathrm{C}} \tag{18}$$

$$a = (1 - \alpha C_{\mathrm{C}})^2 \tag{19}$$

$$a = 1/(1 + \alpha C_{\mathrm{C}}) \tag{20}$$

$$a = 1/(1 + \alpha C_{\mathrm{C}})^2 \tag{21}$$

Zavarukhin and Kuvshinov[86] proposed a mathematical model to describe the kinetics and catalyst deactivation of the formation of nanofibrous carbon from a mixture of methane and hydrogen over a highly loaded nickel catalyst (90 wt% Ni–Al_2O_3) at conversion temperature 490–590 °C and atmospheric pressure. They approximated catalytic activity for coke formation using a parabolic formula as described in eqn (22). A simulation on the model proposed by Nayak *et al.*[87] was done to evaluate the performance of a fluidized catalytic cracking riser reactor using four to ten lump models. The catalyst activity was related to the coke deposition on catalyst using eqn (23). Gao *et al.*[88] proposed an eight-lump kinetic model to estimate the process performance of vacuum residue (VR) catalytic cracking at temperature 460–520 °C and WHSV of 15 h^{-1}. A deactivation expression dependent on the catalyst coke content (C_c) was adopted as shown in eqn (24). Xiong *et al.*[89] developed a novel six-lump kinetic model including catalyst deactivation to determine the cracking performance of a fluidized catalytic cracking process at temperature 460–540 °C, catalyst/oil ration 4–10, and WHSV of 5–30 h^{-1}. The catalytic activity was modeled based on the coking content using eqn (24).

$$a = 1 - \left(\frac{C_{\mathrm{c}}}{C_{\mathrm{c,max}}}\right)^2 \tag{22}$$

$$a = \frac{A + 1}{A + \exp(BC_{\mathrm{c}})} \tag{23}$$

$$a = (1 + \beta C_{\mathrm{c}})^{-m} \tag{24}$$

Barghi and Karimzadeh[90] proposed a kinetic model for the catalytic cracking at 565–635 °C in presence and absence of steam at atmospheric pressure of liquefied petroleum gas (LPG) conversion to olefin and aromatics using ZnO incorporated into a ZSM-5 catalyst. The deactivation model was extended to include coke formation, metal sintering, delamination of the

Open Access Article. Published on 26 July 2023. Downloaded on 1/23/2026 1:45:14 AM.
This article is licensed under a Creative Commons Attribution-NonCommercial 3.0 Unported Licence.

Table 3 Catalyst deactivation dependent on coke formation of fuel and dehydrogenation catalyst systems

Deactivation expression	Catalyst type	TOS	Reactor type	reaction	Reference
$a = \exp(-\alpha C_C)$ $a = 1 - \alpha C_C$ $a = (1 - \alpha C_C)^2$ $a = 1/(1 + \alpha C_C)$ $a = 1/(1 + \alpha C_C)^2$	Cr_2O_3–Al_2O_3	nt[a]	Fixed bed reactor	*i*-Butene dehydrogenation	Dumez and Froment[15]
$a = \dfrac{\alpha}{(1 + \beta t_c{}^{\gamma})P^m}$	FCC catalyst	1.25–5 min	Fluidized dense-bed reactor	Hydrocarbons cracking	Jacob *et al.*[95]
$a = \dfrac{B + 1}{B + \exp(AC_c)}$	nt[a]	20–40 h	Plug flow model	Vacuum gasoil cracking	Martin *et al.*[96]
$a = \dfrac{t_c{}^n}{C_c{}^m}$	Zeolite	0–10 s	Fluidized regenerator and riser cracker	FCC	Arandes and Lasa[60]
$a = \dfrac{B + 1}{B + \exp(AC_c)}$	FCC catalyst	nt[a]	FCC riser reactors	Vacuum gas oil cracking	Nayak *et al.*[87]
$a = \exp(-\alpha C_c)$	Pt–Sn/–Al_2O_3	1–10 day	Tubular quartz reactor	Propane dehydrogenation	Niknaddaf *et al.*[97]
$a = (1 + \beta C_c)^{-m}$	nt[a]	1–40 s	Fluidized bed reactor	Catalytic cracking of vacuum residue	Gao *et al.*[88]
$a = (1 + \alpha C_c)^{-\beta}$	FCC catalyst	nt[a]	Fluidized bed	Catalytic cracking of heavy oil	Xiong *et al.*[89]
$a = A_o \exp(-A_1 C_c)$	Y and ZSM-5	nt[a]	Riser reactor	Vacuum gasoil cracking	Ivanchina *et al.*[91]
$-\dfrac{da}{dt} = k_{do} e^{-\left(\frac{E_d}{RT}\right)} a^n C^m$	CHZ-4	50 min	Fixed bed reactor	Biomass fast pyrolysis oil	Wan *et al.*[93]
$-\dfrac{da}{dt} = k_{do} e^{-\left(\frac{E_d}{RT}\right)} a^n C^m$	Cr_2O_3/Al_2O_3 catalyst	nt[a]	Moving bed reactor	Propane dehydrogenation	Ghodasara, *et al.*[98]
$-\dfrac{da}{dt} = k_{do} e^{-\left(\frac{E_d}{RT}\right)} a^n C^m$	Pd–Ag supported α-Al_2O_3	800 day	Packed bed reactor	Acetylene hydrogenation	Dehghani *et al.*[99]
$a = A_o \exp(-A_1 C_c)$	nt[a]	4.5 s	Plug flow reactor	Catalytic cracking of vacuum distillate and residual feedstock	Nazarova *et al.*[100]
$a = \exp(-K_d t)$ $k_d = k_{do} e^{-\left(\frac{E_d}{RT}\right)}$	Ni/ZrO_2	60 min	Tubular packed-bed reactor	Deoxygenation of palm oil to produce green diesel	Hafeez *et al.*[94]
$a = A_o \exp(-A_1 C_c)$	nt[a]	4.5 s	Riser reactor	Vacuum gasoil cracking	Nazarova *et al.*[17]

[a] Not reported.

zeolite framework and steam effect, and the overall catalyst activity as shown in eqn (25). Ivanchina *et al.*[91] developed a mathematical model for the fluidized catalytic cracking process at 495–542 °C, the pressure is 0.08–0.2 MPa, considering the feedstock composition and catalyst deactivation by coke. The catalytic activity was attributed to primary (a_Y) and secondary ($a_{ZSM\text{-}5}$) reactions during catalytic cracking as described by the exponential dependence in eqn (26) and (27).

$$a = 1 - d_{coke} - d_{sintering} - d_{dealumination} \tag{25}$$

$$a_Y = A_o \exp(-\alpha_1 C_C) \tag{26}$$

$$a_{ZSM\text{-}5} = A_o \exp(-\alpha_2 C_C) \tag{27}$$

The catalyst deactivation model dependent on coke formation cannot predict catalyst activity decay with a high level of accuracy.[92] Table 3 summarizes the most important models attributed to catalyst deactivation including CHZ-4 (ref. 93) and Ni/ZrO_2 (ref. 94) used for biofuels which a dependent on coke formation.

2.4 Reactant dependent catalyst deactivation model

The selective catalyst deactivation was model attributed to an individual effects of the reaction mixture composition, temperature and time (Fig. 2). Gayubo *et al.*[101] proposed a catalyst deactivation expression for methanol-to-olefin (MTO) conversion over ZSM-5 zeolite from coke; the process considered ethylene concentration as a precursor in the temperature

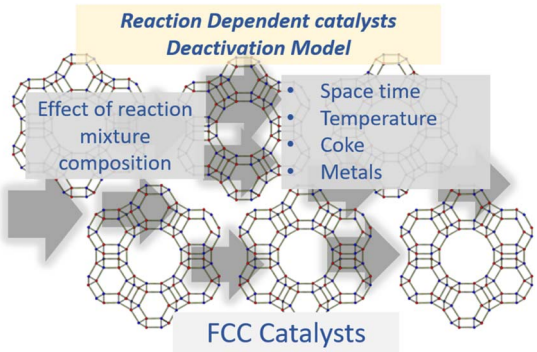

Fig. 2 Selective catalyst deactivation model.

 © 2023 The Author(s). Published by the Royal Society of Chemistry

Open Access Article. Published on 26 July 2023. Downloaded on 1/23/2026 1:45:14 AM.
This article is licensed under a Creative Commons Attribution-NonCommercial 3.0 Unported Licence.

range 400–500 °C. Aguayo *et al.*[102] applied a deactivation model that considered the effect of lump concentration on the coke formation rate at 360–420 °C and contact time between 0.01–0.15 g h^{-1}, over the ZSM-5 zeolite catalyst used for methanol-to-gasoline (MTG) conversion as shown in eqn (28). They demonstrated that the selective deactivation model provided a better representation of the practical results than the empirical model, which did not account for the composition effect upon deactivation.

$$-\frac{da}{dt} = (k_{dA}X_A + k_{dC}X_C + k_{dD}X_D)a \tag{28}$$

Commercial Fischer–Tropsch processes operate at relatively moderate temperatures and pressures. The carbidization, sintering and change of oxidation state cobalt catalysts are the most significant deactivation associated with cobalt-based catalysts.[52] Although Pour *et al.*[30] studied the deactivation kinetics, bulk and nano-structured catalysts prepared by the micro-emulsion method of an iron-based catalyst were applied for Fischer–Tropsch synthesis (FTS). The generalized power-law expression (GPLE), $r_d = k_d(a - a_\infty)^m$ was applied to fit the experimental data of catalyst deactivation rate tested at pressure 17 bar conversion temperature 270–310 °C. Pour *et al.*[103] proposed a different deactivation mechanism to represent the deactivation of a Co-based catalyst supported on carbon nanotubes (CNTs) applied in the Fischer–Tropsch process at pressure 20 bar and temperature 220 °C. They observed that water was the most important deactivating component in Co-based catalysts; therefore, they considered the partial pressure of water in the deactivation kinetic equation. The rate of catalyst deactivation was dependent on the catalyst activity decreasing rate $(a - a_\infty)$ as shown in eqn (29).

$$-\frac{da}{dt} = k_d P_W{}^m (a - a_\infty)^n \tag{29}$$

Centeno *et al.*[104] considered both carbon and metal deposition in a deactivation model to fit the experimental result of different gas oil feedstocks for the hydrotreating process over NiMo/Al oxide in a bench-scale reactor. The experiments were conducted at 380, 400 and 420 °C while sulfur, metal and asphaltene content were analyzed every 10 h during 240 h of time-on-stream (TOS). They observed a good agreement between the experimental and practical deactivation results, whereas the asphaltene content had a significant impact on catalyst deactivation. Table 4 summarizes the most important models for integrating complex catalyst deactivation dependent on coke formation. Similarly, the model has also been applied to ZSM-5 zeolite from coke used for steam catalytic reforming at 550–700 °C and steam/carbon ratio of 1.5–6.0,[105] coke over Ni/Al oxide for catalytic biomass pyrolysis at 600–700 °C and steam/biomass ratio 1.6–12.5, for biofuel production,[106] and CO_2/CO hydrogenation using a Cu–Zn–Zr/SAPO-11 catalyst for the Fischer–Tropsch process at temperature 250–325 °C and 10–50 bar.[107]

2.5 Deactivation model with residual activity

Depending on the mechanism, catalyst deactivation can be reversible or irreversible under various condition.[114] Catalyst deactivation by coke is a reversible process while catalyst

Table 4 Catalyst deactivation dependent on coke formation

Differential form	Catalyst	TOS	Reactor type	Reaction system	Reference
$-\frac{da}{dt} = (k_{dA}X_A + k_{dC}X_C + k_{dD}X_D)a$	HZSM-5 zeolite	10 h	Fixed and fluidized bed reactor	Methanol to gasoline	Aguayo *et al.*[102]
$-\frac{da}{dt} = k_d X_W{}^n a^m$	HZSM-5	2 h	Fixed-bed reactor	Methanol to olefin	Gayubo *et al.*[101]
$-\frac{da}{dt} = k_d P_i{}^n (a - a_{ss})^m$	Fe/Cu/La	105 h	Semi-batch reactor	Fischer–Tropsch	Pour *et al.*[30]
$-\frac{da}{dt} = k_d K_P{}^2 C^2 a^2$	$AuAl_2O_3$	0–440 h	Plug-flow reactor	Pentene isomerization	Solkina *et al.*[108]
$-\frac{da}{dt} = k_d P_W{}^n (a - a_{ss})^m$	Co/CNTs	430 h	Fixed-bed reactor	Fischer–Tropsch	Pour *et al.*[103]
$-\frac{da}{dt} = k_d P_i a^d \theta_d,\ \theta_d = \frac{1}{1 + K_d P_W}$	HZSM-5	18 h	Isothermal fixed bed reactor	Dimethyl ether (DME) to olefins	Pérez-Uriarte *et al.*[109]
$-\frac{da}{dt} = k_d X_{BO}{}^2 a^{2.5}$	HZSM-5	5 h	Fluidized bed reactor	Steam reforming of bio-oil	Gayubo *et al.*[105]
$\frac{da}{dt} = -k_d a^{n1} P_{CH_3OH}{}^{n2}$	Fe–Mo	353 days	Packed bed reactor	Formaldehyde production	Braz *et al.*[110]
$-\frac{da}{dt} = \frac{k_d(P_{DME} + P_{CH_3OH})}{1 + k_{H_2O}P_{H_2O}} a$	$CuO/ZnO/Al_2O_3$	50 h	Fixed-bed reactor	Synthesis of dimethyl ether from syngas	Peláez *et al.*[111]
$-\frac{da}{dt} = k_d x_{C_nH_mO_k} a$	Commercial Ni/Al_2O_3	2 h	Fluidized bed reactor	Biomass pyrolysis	Arregi *et al.*[106]
$-\frac{da}{dt} = a(\alpha P_M + \beta P_A)$	HZSM-5	9–25 h	Fixed-bed reactor	Methanol to aromatic	Li *et al.*[112]
$-\frac{da}{dt} = k_d(P_{MeOH} + P_{DME})\theta_d a$	$CuO–ZnO–ZrO_2$/SAPO-11	48 h	Fixed-bed reactor	CO_2 + CO hydrogenation to dimethyl ether (DME)	Ateka *et al.*[107]
$-\frac{da}{dt} = \beta_1(P_M + 2P_{DME})^{\beta_2} P_A{}^{\beta_3} P_W{}^{-\beta_4} a^{\beta_5}$	HZSM-5	40 h	Fixed-bed reactor	Methanol to olefin	Li *et al.*[113]

Open Access Article. Published on 26 July 2023. Downloaded on 1/23/2026 1:45:14 AM.
This article is licensed under a Creative Commons Attribution-NonCommercial 3.0 Unported Licence.

poisoning by heavy metals (Ni and V) is irreversible.[11] Garetto *et al.*[115] studied the deactivation-regeneration mechanism of a Pt/Al oxide catalyst during hydrodechlorination at temperature 100–130 °C and pressure 2 and 10 bar of carbon tetrachloride. The catalyst deactivation–regeneration model considers the influence of the process operating conditions on catalyst deactivation, as shown in eqn (30), whereas the individual rate of deactivation-regeneration was evaluated using eqn (31) and (32):

$$-\frac{\mathrm{d}a}{\mathrm{d}t} = \psi_{\mathrm{d}} a^{d} - \psi_{\mathrm{r}}\left(a - a^{dm}\right) \tag{30}$$

$$\psi_{\mathrm{d}} = k_{\mathrm{d}} P_{\mathrm{CTC}}{}^{n_{\mathrm{d}}} P_{\mathrm{HH_2}}{}^{m_{\mathrm{d}}} \tag{31}$$

$$\psi_{\mathrm{r}} = k_{\mathrm{r}} P_{\mathrm{CTC}}{}^{n_{\mathrm{r}}} P_{\mathrm{HH_2}}{}^{m_{\mathrm{r}}} \tag{32}$$

Zambrano *et al.*[85] considered five expressions as shown in eqn (33)–(37) to represent the Ni–Ce/Al oxide catalyst deactivation for methane dry reforming with CO_2 at temperature 475–550 °C and space time between 0.5–2 g h mol^{-1}. The best fit was obtained for the residual activity because of the competition between coke formation and coke removal as described in eqn (35).

$$-\frac{\mathrm{d}a}{\mathrm{d}t} = \psi_{\mathrm{d}} a^{d} \tag{33}$$

$$-\frac{\mathrm{d}a}{\mathrm{d}t} = \psi_{\mathrm{d}} a^{d} - \psi_{\mathrm{r}} \tag{34}$$

$$-\frac{\mathrm{d}a}{\mathrm{d}t} = \psi_{\mathrm{d}} a^{d} - \psi_{\mathrm{r}} a^{dm} \tag{35}$$

$$-\frac{\mathrm{d}a}{\mathrm{d}t} = \psi_{\mathrm{d}} a^{m-1/m} - \psi_{\mathrm{r}}\left(a^{1/m} - a_{\mathrm{s}}{}^{1/m}\right)^{h} \tag{36}$$

$$-\frac{\mathrm{d}a}{\mathrm{d}t} = \psi_{\mathrm{d}} a^{d} - \psi_{\mathrm{r}} a^{dm} + \psi_{\mathrm{r}} a \tag{37}$$

Rimaz *et al.*[116] successfully fitted an experimental data on propane conversion over a Pt–Ge/Al oxide catalyst for propane dehydrogenation *vs.* 24 h time-on-stream at 500–600 °C using a deactivation model with residual activity (DMRA) (eqn (38)–(41)).

$$-\frac{\mathrm{d}a}{\mathrm{d}t} = \psi_{\mathrm{d}} a^{3/2} - \psi_{\mathrm{r}} a^{1/2} \tag{38}$$

$$\psi_{\mathrm{d}} = \frac{K_{\mathrm{d1}} P_{\mathrm{CH_4}}{}^{2} + K_{\mathrm{d2}} P_{\mathrm{H_2}}{}^{2} P_{\mathrm{Co}}{}^{2}}{\left(1 + K_{\mathrm{d3}} P_{\mathrm{CO_2}}\right)} \tag{39}$$

$$\psi_{\mathrm{r}} = K_{\mathrm{r1}} P_{\mathrm{CO_2}}{}^{2} \tag{40}$$

$$-\frac{\mathrm{d}a}{\mathrm{d}t} = \psi_{\mathrm{d}} a - \psi_{\mathrm{r}} \sqrt{a} \tag{41}$$

The simplest DMRA model, was used by Cazana *et al.*[117] to express the catalyst activity behavior during the preparation of graphene-related material grown on stainless steel foams at 800–950 °C with methane feed between 3.6–42.9 mol%, *via* the catalytic decomposition of methane, as shown in eqn (42):

$$-\frac{\mathrm{d}a}{\mathrm{d}t} = \psi_{\mathrm{d}} a - \psi_{\mathrm{r}}(1 - a) \tag{42}$$

Gromotka *et al.*[12] integrated three-factor kinetic equations for catalyst deactivation in terms of the apparent kinetic parameters. Three factors were applied: (1) the main catalytic cycle; (2) one-step reversible deactivation; and (3) one-directional irreversible deactivation from organic species accumulation. The obtained equation successfully applied to describe the reversible catalyst deactivation between 150–250 °C during the dehydration of acetaldehyde over a TiO_2 catalyst. Table 5 illustrates the catalyst-deactivation dependent model for a catalyst with residual activity.

Overall, temperature is the most effective variable for the reaction rate, and can be considered the strongest variable affecting the rate of catalysts deactivation or regeneration. Occasionally, as the temperature of an industrial reactor increases, the reaction rate compensates for the decline in catalytic activity caused by the accumulation of coke and metals.[119] Correspondingly, the GPLE is an appropriate deactivation model for cases in which the catalyst activity approaches an asymptotic value over long times such as Fischer–Tropsch

Table 5 Catalyst deactivation dependent with residual activity

Deactivation model	Catalyst	TOS	Reactor type	Reaction system	Reference
$-\frac{\mathrm{d}a}{\mathrm{d}t} = \psi_{\mathrm{d}} a^{d} - \psi_{\mathrm{r}} a^{dm} + \psi_{\mathrm{r}} a$	Commercial silica–alumina	0–90 min	Fixed bed reactor	Isopropyl-benzene cracking	Rodríguez *et al.*[118]
$-\frac{\mathrm{d}a}{\mathrm{d}t} = \psi_{\mathrm{d}} a^{d} - \psi_{\mathrm{r}}(a - a^{dm})$	Pt/Al_2O_3	0–260 min	Fixed-bed tubular reactor	Hydride-chlorination of carbon tetrachloride	Garetto *et al.*[115]
$-\frac{\mathrm{d}a}{\mathrm{d}t} = \psi_{\mathrm{d}} a^{3/2} - \psi_{\mathrm{r}} a^{1/2}$ $\psi_{\mathrm{d}} = \frac{K_{\mathrm{d1}} P_{\mathrm{CH_4}}{}^{2} + K_{\mathrm{d2}} P_{\mathrm{H_2}}{}^{2} P_{\mathrm{Co}}{}^{2}}{\left(1 + K_{\mathrm{d3}} P_{\mathrm{CO_2}}\right)}$ $\psi_{\mathrm{r}} = K_{\mathrm{r1}} P_{\mathrm{CO_2}}{}^{2}$	Ni–Ce/Al_2O_3	4 h	Fixed-bed quartz reactor	Dry reforming of methane	Zambrano *et al.*[85]
$-\frac{\mathrm{d}a}{\mathrm{d}t} = \psi_{\mathrm{d}} a - \psi_{\mathrm{r}}(1 - a)$	Fe nanoparticles	2 h	Fixed bed reactor	Graphene formation by catalytic decomposition of methane	Cazana *et al.*[117]

 © 2023 The Author(s). Published by the Royal Society of Chemistry

Open Access Article. Published on 26 July 2023. Downloaded on 1/23/2026 1:45:14 AM.
This article is licensed under a Creative Commons Attribution-NonCommercial 3.0 Unported Licence.

catalysts at temperature 200–240 °C and pressure 100 bar.[120] The selective deactivation model did not significantly improve the fit of the experimental data.[121] A non-selective deactivation model derived from a simple deactivation kinetic equation for optimum estimation of reaction rates was used to integrate the lumped components in propane aromatization in two zone bed reactors.[119]

3. Mathematical modeling of chemical reactors

Regularly, the mathematical modeling could be classified as deterministic or empirical.[122] The deterministic model is designed from the first-principles equation, while the empirical model is a mathematical expression generalized to fit with chemical reaction data of one or more variables.

3.1 Deterministic models

The deterministic model involves solving a system of ordinary differential equations for chemical reactions to estimate process performance. Accurate kinetic and catalyst deactivation models are crucial for the modeling, optimization, and part of chemical reactors control. The rigorous dynamic mathematical model of a reactor consists of solving nonlinear simultaneous equations (algebraic, differential and sometimes partial) in multiple dependent variables (product concentrations, coke content, temperature and pressure). The reactants and product distribution in reaction mixture can be estimated by solving the kinetic model equations. The dynamic coke content can be updated by integrating the corresponding differential equation describing the coke formation in time domain, the catalyst activity is easily related to time, product distribution and coke content using either algebraic or differential form of the catalyst deactivation model. The heat balance equation designed to estimate the temperature of the reaction mixture with respect to time, while Arrhenius equation is usually used to estimate the change of reaction rate and deactivation rate constants as a function of temperature. In the case of the heterogeneous fixed bed reactor model, the differential format of Ergun's equation can be integrated to calculate the pressure drop within the reactor bed. For gaseous reactions the reaction rate can be related to the partial pressures of reactants using at least one of the approved reaction mechanisms (Power law, Eley–Rideal, and Langmuir–Hinshelwood). This set of highly coupled nonlinear differential equations describes the reactants and product distribution, coke content, catalyst deactivation temperature and pressure are integrated through the reactor system. The detailed system of ordinary differential equations (ODEs) intents to capture the dynamic changes over time. Therefore, the ordinary differential equation (ODE) governing the rate of change in catalyst activity is projected to be solved simultaneously the change in the reaction conditions under different pressures and temperatures along with the compositions of the reaction mixture. Accordingly, the non-linear interference is bound by the catalyst activity, operating conditions and composition of the reaction mixture.[20,123]

Table 6 The error evaluation expressions[125]

Error function	Expression
Correlation coefficient of determination (R^2)	$1-\frac{\sum_{i=1}^{N}(y_{\mathrm{exp},i}-y_{\mathrm{pred},i})^2}{\sum_{i=1}^{N}(y_{\mathrm{exp},i}-\overline{y}_{\mathrm{exp}})^2}$
Mean absolute error (MAE)	$\frac{1}{N\times M}\sum_{j=1}^{M}\sum_{i=1}^{N}\left\lvert y_{i,j}^{\mathrm{exp}}-y_{i,j}^{\mathrm{pred}}\right\rvert$
Mean relative error (MRE)	$\frac{1}{N\times M}\sum_{j=1}^{M}\sum_{i=1}^{N}\left(\frac{y_{i,j}^{\mathrm{exp}}-y_{i,j}^{\mathrm{pred}}}{y_{i,j}^{\mathrm{exp}}}\right)$
Mean square error (MSE)	$\frac{1}{N\times M}\sum_{j=1}^{M}\sum_{i=1}^{N}(y_{i,j}^{\mathrm{exp}}-y_{i,j}^{\mathrm{pred}})$

These differential equations usually describe the fourth-order Runge–Kutta integration method. The kinetic and deactivation parameters were obtained by benchmarking the experimental and predicted results using a stochastic optimization method. Similarly, the optimization methods applied an artificial neural network (ANN), Genetic Algorithm (GA) and Particle Swarm Optimization (PSO).[124] These optimization methods were designed iteratively to estimate the best kinetic and deactivation parameters which were expected to yield the minimum error between the experimental and predicted

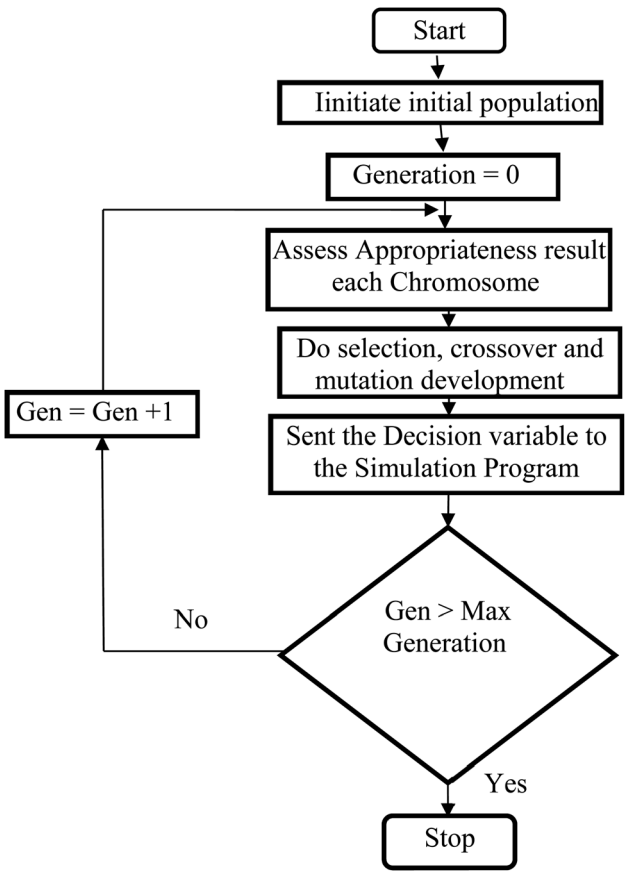

Fig. 3 Genetic Algorithm (GA) computational procedure.

Open Access Article. Published on 26 July 2023. Downloaded on 1/23/2026 1:45:14 AM.
This article is licensed under a Creative Commons Attribution-NonCommercial 3.0 Unported Licence.

results. The widely used error evaluation expressions are presented as listed in Table 6.

Where; $y_{i,j}$ is the mole fraction of ith component in jth experiments, M represents the number of experiments, N is the number of components, exp. and pred. are the superscripts denoting the experimental and predicted results, respectively.

Genetic algorithms (GA) are powerful stochastic optimization method which is designed for the natural selection and natural evaluation concepts.[126] A GA applies to a population of individuals presents a selected solution to the optimization complication. Therefore, the individuals are comprised of strings or chromosomes of genes, the genes, are practical allele. GAs applies the principles of survival of the fittest, selection, reproduction, crossover, and mutation to these individuals to obtain a new better individual for each new solution.[127,128] Genetic Algorithm creates a new chromosomes population by choosing better-fit results obtained from the existing population and applying genetic operators to produce new offspring from the result. The algorithm for Genetic Algorithm stochastic optimization method is depicted in Fig. 3.

3.2 Artificial neural network (ANN) model

The kinetic parameters of catalyst deactivation (k_{do} and E_{da}) can be estimated empirically by fitting the response of the reaction mixture with respect to time and other effective variables. The activity at reaction start will be 100% initially and it decays with time. Therefore, the same catalyst has different deactivation kinetic parameters (k_{do} and E_{da}) for different reaction systems. For the same catalyst and the same initial activity, solving the deactivation kinetic models having different kinetic parameters will produce different deactivation responses. In case of the rigorous mathematical modeling of chemical reactors, the effect of time, reactant, poison, and products on the catalyst activity can be represented using an appropriate selective deactivation model. Recently, using artificial intelligence (AI) aims to capture the effect of any different input variables on the product distribution, catalyst activity and reaction temperatures. The artificial neural network (ANN) model designed to have the ability to establish relationships between multiple input–output variables. Artificial neural networks (ANNs) mimics the processes of the human brain and are series of mathematical algorithms that used in this study to estimate the relationships between datasets.[129,130] ANNs models can intgerate empirical relationships between dependent and independent variables based on experimental data. The ANN contains several layers; an input layer, a hidden layer, and an output layer as shown in Fig. 4.

ANNs are utilized to predict variables processed in a rapid manner and provide precise prediction under a complex process. ANNs are broadly applied for modeling and controlling multipart of chemical reactors and processes to accurately simulate atmospheric distillation columns,[131,132] various of heat exchangers,[133,134] and catalytic reactors.[135,136] Approximation of the reaction rate obtained without a kinetic model would

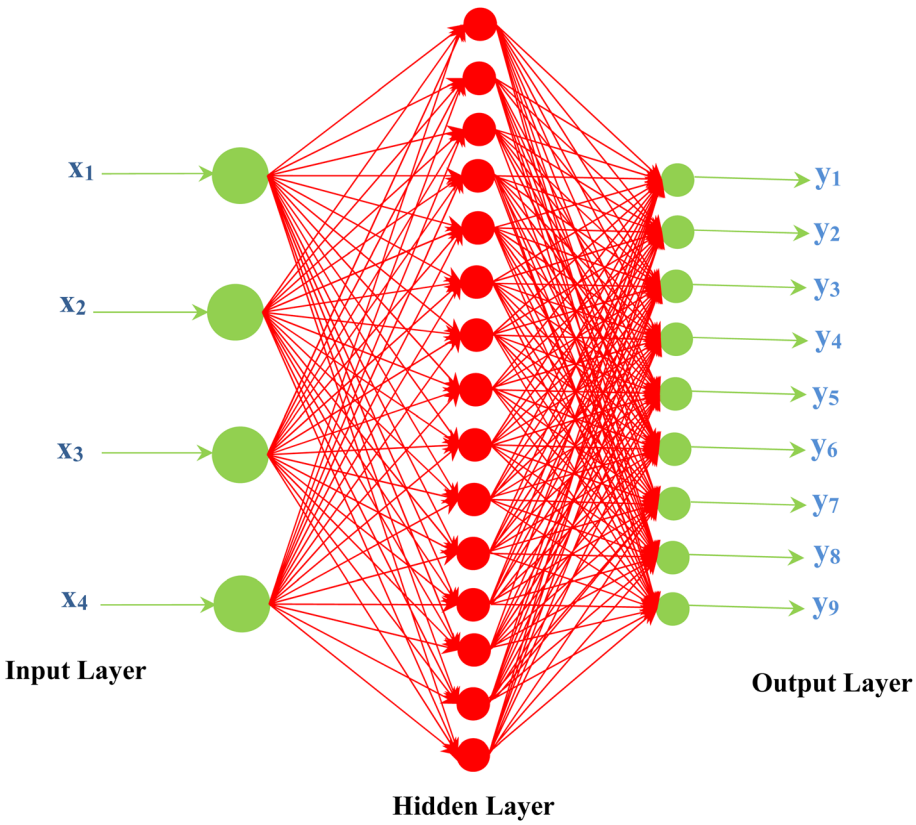

Fig. 4 The neural network (ANN) with three layers.

 © 2023 The Author(s). Published by the Royal Society of Chemistry

Open Access Article. Published on 26 July 2023. Downloaded on 1/23/2026 1:45:14 AM.
This article is licensed under a Creative Commons Attribution-NonCommercial 3.0 Unported Licence.

eliminate the errors obtained from choosing of the kinetic method related to the catalyst deactivation models for kinetic constant integration.[137]

4. Conclusion

Catalyst deactivation is a complex phenomenon, and an appropriate deactivation model is essential for process design and control to maximize catalyst utilization and maintain the catalytic production. Several mathematical models have been highlighted in the literature to describe catalyst deactivation in different reaction systems and operating conditions. Deactivation models play a significant role in the simulation, optimization and design of chemical catalytic reactors. This study considered scientific narratives to comprehend different catalyst deactivation models. From this review the following conclusions were drawn:

• The time dependent deactivation model is appropriate for systems with fast catalyst deactivation such as fluidized catalytic cracking, because the catalyst activity depends more on the effects of the deactivation rate over time than on temperature and reactant concentrations.

• For the dynamic process, the differential form of catalyst deactivation is slightly more accurate than the algebraic form; hence it represents the instantaneous catalyst activity in a dynamic system.

• The generalized power-law equation (GPLE) is a powerful equation for a long-term deactivation process.

• Selective deactivation kinetic models are limited because they are often complex and difficult to integrate.

Abbreviations

A, B, r, α, β	Deactivation constants
A_a	Pre-exponential factor (mol^{-1} L h^{-1})
A_d	Deactivation of pre-exponential factor (mol^{-1} L h^{-1})
a	Activity of catalyst (−)
a_∞	Catalyst activity infinite reaction time
C_c	Coke content on the catalyst (wt%.)
C_i	Concentration of the ith component (mol l^{-1})
E_a	Activation energy of the reaction (kJ mol^{-1})
E_d	Deactivation energy (kJ mol^{-1})
k_d	Deactivation rate constant [h^{-1}]
k_r	Regeneration rate constant [h^{-1}]
k_{d0}	Pre-exponential factors, [g $cm^{-3}]^{-1}$ h^{-1}
m, n	Activity term power
P	Reaction pressure (Pa)
P_i	Partial pressure of species I (Pa)
R	Gas constant 8.31451 (J mol^{-1} K^{-1})
T	Reaction temperature (K)
T_o	Reference temperature (K)
TOS	Time on stream (h)
t	Time (h)
t_R	Residence time (h)
X_i	Weight fraction of lump I (wt%.)
α_1 and α_2	Catalyst deactivation constants
θ	Term that quantifies the attenuation of the reaction rates by the adsorption
ψ_d	Deactivation kinetic function
ψ_r	Regeneration kinetic function

Subscripts

A, C and D	Indicate to oxygenates (methanol and dimethylether), light olefins (ethylene and propylene) and lump of the rest of hydrocarbons respectively
BO	Bio-oil
DME	De-methyl ether
max	Maximum
MeOH	Methanol
W	Water
∞	Infinity

Conflicts of interest

The authors declare no competing financial interest.

Acknowledgements

The author would like to acknowledge the scientific support from the Department of Chemical Engineering, University of Technology, Baghdad, Iraq.

References

1 A. S. Krishna, *Catal. Rev.: Sci. Eng.*, 1990, **32**(4), 279–381.
2 G. C. Hadjiloizou, J. B. Butt and J. S. Dranoff, *J. Catal.*, 1992, **135**(1), 27–44.
3 S. Ordóñez, P. Hurtado, H. Sastre and F. V. Diez, *Appl. Catal., A*, 2004, **259**(1), 41–48.
4 L. W. Jossens and E. E. Petersen, *J. Catal.*, 1982, **76**(2), 265–273.
5 S. Hamoudi, K. Belkacemi and F. Larachi, *Chem. Eng. Sci.*, 1999, **54**(15–16), 3569–3576.
6 A. Monzón, E. Romeo and A. Borgna, *Chem. Eng. J.*, 2003, **94**(1), 19–28.
7 Z. Ke, Z. Ya-ping, H. Tian-jiao, L. Bin and S. Kai, *J. Fuel Chem. Technol.*, 2017, **45**(11), 1356–1364.
8 J. Schirme, J. S. Kim and E. Klemm, *J. Anal. Appl. Pyrolysis*, 2001, **60**(2), 205–217.
9 J. Ogonowski and E. Skrzyńska, *Catal. Lett.*, 2008, **121**(3–4), 234–240.
10 A. Morris and C. Bartholomew, *Catalysts*, 2015, **5**(1), 145–269.
11 C. Bartholomew, *Appl. Catal., A*, 2001, **212**, 17–60.
12 Z. Gromotka, G. Yablonsky, N. Ostrovskii and D. Constales, *Entropy*, 2021, **23**(7), 818.
13 A. Voorhies Jr, *Ind. Eng. Chem.*, 1945, **37**(4), 318–322.
14 V. W. Weekman Jr, *Ind. Eng. Chem. Process Des. Dev.*, 1968, **7**(1), 90–95.

Open Access Article. Published on 26 July 2023. Downloaded on 1/23/2026 1:45:14 AM.
This article is licensed under a Creative Commons Attribution-NonCommercial 3.0 Unported Licence.

15 F. J. Dumez and G. F. Froment, *Ind. Eng. Chem. Process Des. Dev.*, 1976, **15**(2), 291–301.
16 K. R. Devoldere and G. F. Froment, *Ind. Eng. Chem. Res.*, 1999, **38**(7), 2626–2633.
17 G. Nazarova, E. Ivashkina, E. Ivanchina, A. Oreshina, I. Dolganova and M. Pasyukova, *Fuel Process. Technol.*, 2020, **200**, 106318.
18 A. A. Ebrahimi, H. Mousavi, H. Bayesteh and J. Towfighi, *Fuel*, 2018, **231**, 118–125.
19 T. Cordero-Lanzac, A. T. Aguayo, A. G. Gayubo, P. Castaño and J. Bilbao, *Chem. Eng. J.*, 2020, **379**, 122260.
20 Z. M. Shakor, A. A. AbdulRazak and K. A. Sukkar, *Arabian J. Sci. Eng.*, 2020, **45**(9), 7361–7370.
21 C. H. Bartholomew, *Catalyst Deactivation in Hydrotreating of Residua: A Review*, Marcel Dekker, New York, 1994.
22 H. O. Otor, J. B. Steiner, C. Garcia-Sancho and A. C. Alba-Rubio, *ACS Catal.*, 2020, **10**(14), 7630–7656.
23 A. Ochoa, J. Bilbao, A. G. Gayubo and P. Castaño, *Renewable Sustainable Energy Rev.*, 2020, **119**, 109600.
24 J. Zhou, J. Zhao, J. Zhang, T. Zhang, M. Ye and Z. Liu, *Chin. J. Catal.*, 2020, **41**(7), 1048–1061.
25 A. Szymaszek, B. Samojeden and M. Motak, *Energies*, 2020, **13**(15), 3870.
26 G. F. Froment, Modeling of catalyst deactivation, *Appl. Catal., A*, 2001, **212**(1–2), 117–128.
27 P. U. Okoye, A. Z. Abdullah and B. H. Hameed, *Renewable Sustainable Energy Rev.*, 2017, **74**, 387–401.
28 I. Elizalde and J. Ancheyta, *Fuel Process. Technol.*, 2014, **123**, 114–121.
29 T. M. Moustafa and G. F. Froment, *Ind. Eng. Chem. Res.*, 2003, **42**(1), 14–25.
30 A. N. Pour, M. R. Housaindokht, S. F. Tayyari, J. Zarkesh and M. R. Alaei, *J. Mol. Catal. A: Chem.*, 2010, **330**(1–2), 112–120.
31 V. N. Parmon and N. M. Ostrovskii, *React. Kinet., Mech. Catal.*, 2020, **131**(1), 37–55.
32 M. L. Occelli, *Fluid Catalytic Cracking 2*, American Chemical Society, Washington, DC, United States, 1991.
33 Y. Ozawa, Y. Tochihara, M. Nagai and S. Omi, *Chem. Eng. Sci.*, 2003, **58**(3–6), 671–677.
34 J. Markos, A. Brunovska and J. Ilavsky, *Chem. Pap.*, 1987, **41**, 375.
35 K. N. Theologos and N. C. Markatos, *AIChE J.*, 1993, **39**(6), 1007–1017.
36 D. R. Rainer, E. Rautiainen and P. Imhof, *Appl. Catal., A*, 2003, **249**(1), 69–80.
37 O. A. Olafadehan, O. P. Sunmola, A. Jaiyeola, V. Efeovbokhan and O. G. Abatan, *Appl. Petrochem. Res2E*, 2018, **8**, 219–237.
38 R. Zhang, L. Li, Z. Liu and X. Meng, *Int. J. Chem. Eng.*, 2016, **2016**, 9148925.
39 T. P. Jadon, A. K. Jana and P. Parikh, *Biomass Convers. Biorefin.*, 2021, **11**, 1093–1099.
40 G. Trunfio and F. Arena, *Catalysts*, 2014, **4**(2), 196–214.
41 P. Hagelberg, I. Eilos, J. Hiltunen, K. Lipiäinen, V. M. Niemi, J. Aittamaa and A. O. Krause, *Appl. Catal., A*, 2002, **223**(1–2), 73–84.
42 A. Ricca, F. Montella, G. Iaquaniello, E. Palo, A. Salladini and V. Palma, *Catal. Today*, 2019, **331**, 43–52.
43 D. V. Naik, V. Karthik, V. Kumar, B. Prasad and M. O. Garg, *Chem. Eng. Sci.*, 2017, **170**, 790–798.
44 F. T. Zangeneh, A. Taeb, K. Gholivand and S. Sahebdelfar, *J. Energy Chem.*, 2013, **22**(5), 726–732.
45 D. Sun, F. M. Khan and D. S. Simakov, *Chem. Eng. J.*, 2017, **329**, 165–177.
46 A. G. Sani, H. A. Ebrahim and M. J. Azarhoosh, *Fuel*, 2018, **225**, 322–335.
47 Y. Lin, Y. Wang, W. Feng, G. Wu, J. Xu, T. Zhang, S. Wang, X. Wu and P. Yao, *React. Kinet., Mech. Catal.*, 2014, **112**, 267–282.
48 R. B. Demuner, J. G. Soares Santos Maia, A. R. Secchi, P. A. Melo, R. W. do Carmo and G. S. Gusmão, *Ind. Eng. Chem. Res.*, 2019, **58**(8), 2717–2726.
49 M. T. Ravanchi, S. Sahebdelfar, M. R. Fard, S. Fadaeerayeni and P. Bigdeli, *Chem. Eng. Technol.*, 2016, **39**(2), 301–310.
50 Q. Chen and A. C. Lua, *Chem. Eng. J.*, 2020, **389**, 124366.
51 C. H. Bartholomew, *Appl. Catal., A*, 1993, **107**(1), 1–57.
52 M. D. Argyle, T. S. Frost and C. H. Bartholomew, *Top. Catal.*, 2014, **57**, 415–429.
53 J. Ruelas-Leyva and G. Fuentes, *Catalysts*, 2017, **7**(7), 193.
54 M. Ghofran Pakdel, H. Atashi, H. Zohdi-Fasaei and A. A. Mirzaei, *Pet. Sci. Technol.*, 2019, **37**(5), 500–505.
55 N. M. Ostrovskii, *Chem. Eng. J.*, 2006, **120**(1–2), 73–82.
56 L. Honken, Optimization of methanol reactor, *Master Thesis*, Department of Chemical Engineering, Norwegian University of Science and Technology, 1995.
57 H. Kordabadi and A. Jahanmiri, *Chem. Eng. Process.*, 2007, **46**(12), 1299–1309.
58 M. Farsi and A. Jahanmiri, *J. Nat. Gas Chem.*, 2012, **21**(4), 407–414.
59 M. Farsi and A. Jahanmiri, *J. Ind. Eng. Chem.*, 2014, **20**(5), 2927–2933.
60 J. M. Arandes and H. I. Lasa, *Chem. Eng. Sci.*, 1992, **47**(9–11), 2535–2540.
61 E. Rodríguez, G. Elordi, J. Valecillos, S. Izaddoust, J. Bilbao, J. M. Arandes and P. Castaño, *Fuel Process. Technol.*, 2019, **192**, 130–139.
62 C. Seidel, A. Jörke, B. Vollbrecht and A. Seidel-Morgenstern, *Comput.-Aided Chem. Eng.*, 2018, **43**, 85–90.
63 S. Masoudi, M. Farsi and M. R. Rahimpour, *Oil Gas Sci. Technol.*, 2019, **74**, 90.
64 M. R. Rahimpour, D. Iranshahi and A. M. Bahmanpour, *Int. J. Hydrogen Energy*, 2010, **35**(14), 7498–7511.
65 S. Ewald, M. Kolbeck, T. Kratky, M. Wolf and O. Hinrichsen, *Appl. Catal., A*, 2019, **570**, 376–386.
66 S. S. Arumugamurthy, P. Sivanandi, S. Pandian, H. Choksi and D. Subramanian, *Waste Manage.*, 2019, **100**, 318–326.
67 J. Martínez and J. Ancheyta, *Fuel*, 2012, **100**, 193–199.
68 D. Iranshahi, E. Pourazadi, K. Paymooni, A. M. Bahmanpour and M. R. Rahimpour, *Int. J. Hydrogen Energy*, 2010, **35**(23), 12784–12799.
69 M. R. Usman, D. L. Cresswell and A. A. Garforth, *Int. Scholarly Res. Not.*, 2013, **2013**, 152893.

 © 2023 The Author(s). Published by the Royal Society of Chemistry

Open Access Article. Published on 26 July 2023. Downloaded on 1/23/2026 1:45:14 AM.
This article is licensed under a Creative Commons Attribution-NonCommercial 3.0 Unported Licence.

70 H. Xu, J. Si and G. Luo, *Int. J. Chem. React. Eng.*, 2017, **15**(4), 20160165.
71 W. Feng, Y. Wang, G. Wu, Y. Lin, J. Xu, H. Shi, T. Zhang, S. Wang, X. Wu and P. Yao, *J. Chem. Technol. Biotechnol.*, 2015, **90**(8), 1489–1496.
72 N. Taufiqurrahmi, A. R. Mohamed and S. Bhatia, *Chem. Eng. J.*, 2010, **163**(3), 413–421.
73 Z. Li, W. Zhong, X. Wang, N. Luo and F. Qian, *Comput. Chem. Eng.*, 2016, **88**, 1–2.
74 S. M. Jokar, P. Parvasi and A. Basile, *Int. J. Hydrogen Energy*, 2019, **44**(47), 25730–25739.
75 E. A. Morosanu, F. Salomone, R. Pirone and S. Bensaid, *Catalysts*, 2020, **10**(3), 283.
76 I. Pala-Rosas, J. L. Contreras, J. Salmones, B. Zeifert, R. López-Medina, J. Navarrete-Bolaños, S. Hernández-Ramírez, J. Pérez-Cabrera and A. A. Fragoso-Montes de Oca, *Catalysts*, 2021, **11**(3), 360.
77 M. Larsson, M. Hultén, E. A. Blekkan and B. Andersson, *J. Catal.*, 1996, **164**(1), 44–53.
78 M. Larsson, N. Henriksson and B. Andersson, *Stud. Surf. Sci. Catal.*, 1997, **111**, 673–680.
79 M. T. Shah, R. P. Utikar, V. K. Pareek, G. M. Evans and J. B. Joshi, *Chem. Eng. Res. Des.*, 2016, **111**, 403–448.
80 G. F. Froment, *Curr. Opin. Chem. Eng.*, 2014, **5**, 1–6.
81 F. López-Isunza, *Stud. Surf. Sci. Catal.*, 2001, **134**, 187–199.
82 P. Varshney, D. Kunzru and S. K. Gupta, *Indian Chem. Eng.*, 2015, **57**(2), 115–135.
83 J. Corella and J. M. Asua, *Ind. Eng. Chem. Process Des. Dev.*, 1982, **21**(1), 55–61.
84 J. Corella, J. Adanez and A. Monzon, *Ind. Eng. Chem. Res.*, 1988, **27**(3), 375–381.
85 D. Zambrano, J. Soler, J. Herguido and M. Menéndez, *Top. Catal.*, 2019, **62**, 456–466.
86 G. F. Froment and K. B. Bischoff, *Chem. Eng. Sci.*, 1961, **16**(3–4), 189–201.
87 S. V. Nayak, S. L. Joshi and V. V. Ranade, *Chem. Eng. Sci.*, 2005, **60**, 6049–6066.
88 H. Gao, G. Wang, C. Xu and J. Gao, *Energy Fuels*, 2014, **28**(10), 6554–6562.
89 K. Xiong, C. Lu, Z. Wang and X. Gao, *Fuel*, 2015, **161**, 113–119.
90 B. Barghi and R. Karimzadeh, *React. Kinet., Mech. Catal.*, 2017, **120**, 753–773.
91 E. Ivanchina, E. Ivashkina and G. Nazarova, *Chem. Eng. J.*, 2017, **329**, 262–274.
92 A. Haghlesan, R. Alizadeh and E. Fatehifar, *Pet. Sci. Technol.*, 2016, **34**(6), 499–504.
93 L. Wan, S. P. Zhang, S. T. Zhao, Q. L. Xu and Y. J. Yan, *Energy Sources, Part A*, 2013, **35**(9), 800–808.
94 S. Hafeez, S. M. Al-Salem, K. N. Papageridis, N. D. Charisiou, M. A. Goula, G. Manos and A. Constantinou, *Catalysts*, 2021, **11**(6), 747.
95 S. M. Jacob, B. Gross, S. E. Voltz and V. W. Weekman Jr, *AIChE J.*, 1976, **22**(4), 701–713.
96 M. P. Martin, C. Derouin, P. Turlier, M. Forissier, G. Wild and J. R. Bernard, *Chem. Eng. Sci.*, 1992, **47**(9–11), 2319–2324.
97 S. Niknaddaf, M. Soltani, A. Farjoo and F. Khorasheh, *Pet. Sci. Technol.*, 2013, **31**(23), 2451–2462.
98 K. Ghodasara, S. Hwang and R. Smith, *Korean J. Chem. Eng.*, 2015, **32**, 2169–2180.
99 O. Dehghani, M. Rahimpour and A. Shariati, *Processes*, 2019, **7**(3), 136.
100 G. Y. Nazarova, E. N. Ivashkina, E. D. Ivanchina, A. V. Vosmerikov, L. N. Vosmerikova and A. V. Antonov, *Catalysts*, 2021, **11**(6), 701.
101 A. G. Gayubo, A. T. Aguayo, M. Olazar, R. Vivanco and J. Bilbao, *Chem. Eng. Sci.*, 2003, **58**(23–24), 5239–5249.
102 A. T. Aguayo, A. G. Gayubo, J. Ortega, M. Olazar and J. Bilbao, *Catal. Today*, 1997, **37**(3), 239–248.
103 A. A Nakhaei Pour, E. Hosaini and M. Feyzi, *J. Iran. Chem. Soc.*, 2016, **13**, 139–147.
104 G. Centeno, J. Ancheyta, A. Alvarez, G. Marroquín, F. Alonso and A. Castillo, *Fuel*, 2012, **100**, 73–79.
105 A. G. Gayubo, B. Valle, B. Aramburu, C. Montero and J. Bilbao, *Chem. Eng. J.*, 2018, **332**, 192–204.
106 A. Arregi, G. Lopez, M. Amutio, I. Barbarias, L. Santamaria, J. Bilbao and M. Olazar, *Int. J. Hydrogen Energy*, 2018, **43**(27), 12023–12033.
107 A. Ateka, M. Sanchez-Contador, A. Portillo, J. Bilbao and A. T. Aguayo, *Fuel Process. Technol.*, 2020, **206**, 106434.
108 Y. S. Solkina, S. I. Reshetnikov, M. Estrada, A. Simakov, D. Y. Murzin and I. L. Simakova, *Chem. Eng. J.*, 2011, **176**, 42–48.
109 P. Pérez-Uriarte, A. Ateka, A. G. Gayubo, T. Cordero-Lanzac, A. T. Aguayo and J. Bilbao, *Chem. Eng. J.*, 2017, **311**, 367–377.
110 C. G. Braz, A. Mendes, J. Rocha, R. Alvim and H. Matos, *Chem. Eng. Sci.*, 2019, **195**, 347–355.
111 R. Peláez, E. Bryce, P. Marín and S. Ordóñez, *Fuel Process. Technol.*, 2018, **179**, 378–386.
112 H. Li, X. G. Li and W. D. Xiao, *RSC Adv.*, 2019, **9**(39), 22327–22335.
113 X. G. Li, X. Huang, Y. L. Zhang, H. Li, W. D. Xiao and Z. Wei, *Chem. Eng. Sci.*, 2020, **226**, 115859.
114 M. Guisnet, and F. R. Ribeiro, *Deactivation and regeneration of zeolite catalysts*, Catalytic Science Series, Imperial College Press, London, 2011, vol. 9.
115 T. F. Garetto, C. I. Vignatti, A. Borgna and A. Monzón, *Appl. Catal., B*, 2009, **87**(3–4), 211–219.
116 S. Rimaz, L. Chen, A. Monz, S. Kawi and A. Borgna, *Chem. Eng. J.*, 2021, **405**, 126656.
117 F. Caznana, N. Latorre, P. Tarifa, C. J. Royo, V. Sebastián, E. Romeo, M. A. Centeno and A. Monzón, *Catal. Today*, 2022, **383**, 236–246.
118 J. C. Rodríguez, J. A. Peña, A. Monzón, R. Hughes and K. Li, *Chem. Eng. J. Biochem. Eng. J.*, 1995, **58**(1), 7–13.
119 M. P. Gimeno, J. Soler, J. Herguido and M. Menéndez, *Ind. Eng. Chem. Res.*, 2010, **49**(3), 996–1000.
120 S. A. Eliason and C. H. Bartholomew, *Appl. Catal., A*, 1999, **186**(1–2), 229–243.
121 J. Corella, *Ind. Eng. Chem. Res.*, 2004, **43**(15), 4080–4086.
122 A. Al-Shathr, Z. M. Shakor, H. S. Majdi, A. A. AbdulRazak and T. M. Albayati, *Catalysts*, 2021, **11**(9), 1034.

Open Access Article. Published on 26 July 2023. Downloaded on 1/23/2026 1:45:14 AM.
This article is licensed under a Creative Commons Attribution-NonCommercial 3.0 Unported Licence.

123 A. Al-Shathr, Z. M. Shakor, B. Y. Al-Zaidi, H. S. Majdi, A. A. AbdulRazak, S. Aal-Kaeb, A. A. Shohib and J. McGregor, *Int. J. Chem. Eng.*, 2022, **2022**, 8303874.
124 A. Anand and L. Suganthi, *Energies*, 2018, **11**(4), 728.
125 S. J. Kim, S. J. Bae and M. W. Jang, *Sustainability*, 2022, **14**(18), 11674.
126 Z. M. Shakor and A. H. Sadeiq, *Eng. Technol. J.*, 2018, **36**(11A), 1171–1175.
127 R. H. Saihod, Z. M. Shakoor and A. A. Jawad, *Al-Khawarizmi Eng. J.*, 2014, **10**(1), 47–61.
128 S. Mirjalili, J. S. Dong, A. S. Sadiq and H. Faris, *Nature-Inspired Optimizers: Theories, Literature Reviews and Applications*, 2020, pp. 69–85.
129 D. Galvan, H. Cremasco, A. C. Mantovani, E. Bona, M. Killner and D. Borsato, *Fuel*, 2020, **267**, 117221.
130 X. Y. Tai, R. Ocone, S. D. Christie and J. Xuan, *Energy AI*, 2022, **7**, 100134.
131 Á. Ibarra, I. Hita, J. M. Arandes and J. Bilbao, *Catalysts*, 2020, **10**(10), 1157.
132 F. Schmutzler, C. Zschiesche, J. Titus, D. Poppitz, J. Freiding, R. Rakoczy, A. Reitzmann and R. Gläser, *Chem. Ing. Tech.*, 2021, **93**(6), 981–989.
133 M. O. Kazakov, M. Y. Smirnova, M. E. Dubinin, T. S. Bogomolova, P. P. Dik, I. S. Golubev, M. E. Revyakin, O. V. Klimov and A. S. Noskov, *Fuel*, 2023, **344**, 128085.
134 J. M. Schweitzer, J. Rey, C. Bignaud, T. Bučko, P. Raybaud, M. Moscovici-Mirande, F. Portejoie, C. James, C. Bouchy and C. Chizallet, *ACS Catal.*, 2022, **12**(2), 1068–1081.
135 W. Song, V. Mahalec, J. Long, M. Yang and F. Qian, *Ind. Eng. Chem. Res.*, 2020, **59**(7), 3077–3090.
136 B. D. Vandegehuchte, J. W. Thybaut, A. Martinez, M. A. Arribas and G. B. Marin, *Appl. Catal., A*, 2012, **441**, 10–20.
137 D. Baş, F. C. Dudak and I. H. Boyacı, *J. Food Eng.*, 2007, **79**(2), 622–628.

 © 2023 The Author(s). Published by the Royal Society of Chemistry